Northumbria Research Link

Northumbria
University
NEWCASTLE

UniversityLibrary

Analysis of Nyquist Pulse Shapes for Carrier-less Amplitude and Phase Modulation in Visible Light Communications

Paul Anthony Haigh, Petr Chvojka, Stanislav Zvanovec, Zabih Ghassemlooy and Izzat Darwazeh

Abstract—This paper proposes and experimentally demonstrates, for the first time, two new candidate pulse shapes for carrier-less amplitude and phase modulation in the context of visible light communications. It is commonly accepted that the pulse shape at the heart of the Hilbert pair used to generate the required orthogonal signal spaces should be the square-root raised cosine. In this work, we introduce two additional candidate pulse shapes, namely the first-order Xia pulse and the so-called better-than-Nyquist pulse. We demonstrate experimentally that the better-than-Nyquist pulse offers superior bit-error rate performance compared to the square-root raised cosine and Xia pulses under additive white Gaussian noise channel conditions, whilst offering lower computational complexity.

Index Terms—Carrier-less amplitude and phase modulation, digital signal processing, modulation formats, pulse shaping, visible light communications.

I. Introduction

IN visible light communications (VLC), relatively high data rates in the Gb/s region have been presented in the literature [1–3]. Furthermore, highly spectrally efficient modulation formats have been proposed recently, including the well established orthogonal frequency division multiplexing (OFDM) [1] and carrier-less amplitude and phase modulation (CAP) [2, 4]. In a comparative study performed in [2], CAP modulation was shown to outperform OFDM over the same physical link, supporting a data rate of ∼3.22 Gb/s, in comparison to the ∼2.93 Gb/s available with OFDM, with the bit-error rate (BER) of both being approximately 10^{-4} [2]. On the other hand, the additional 10% data rate improvement comes at the cost of system complexity as CAP is generated using two finite impulse response (FIR) filters at the transmitter (one each for the in-phase and the quadrature), and two corresponding matched FIR filters at the receiver [5, 6].

Traditionally in CAP, the shapes of the pulses that form the impulse responses of the transmit filters are the product of a square root raised cosine (SRRC) and a sinusoidal carrier.

Such an approach has been used since the first reports of CAP, i.e. [7], because it provides a pulse that satisfies the first Nyquist criterion for zero inter-symbol interference (ISI) when used in matched filter form, or simply as a full raised cosine. Since the conception of CAP by Falconer in 1975 [8], there have been numerous pulses proposed for pulse shaping in single-carrier modulation formats as reported in [9], which have not been tested in VLC. Several of these pulse shapes can even be considered as improved candidates for the CAP impulse basis function, such as the Xia pulse [10] and the so-called better-than-Nyquist (BTN) [11] pulse, both selected for test in this work.

The reason we decided to implement and analyse these two pulses is as follows. The Xia pulse is asymmetrical, where more energy exists before the peak than after it, whilst still satisfying the Nyquist first criterion for zero ISI [10]. This introduces an interesting characteristic because the FIR filters adopted in a digital implementation of CAP are computationally demanding as the number of operations increases linearly with the filter length and this has an impact on the link BER performance [12, 13]. Thus, if asymmetrical clipping of the filter could be achieved without a significant impact on the BER performance, this would be advantageous. The first analysis of Xia-based CAP (X-CAP) was reported in [14], showing slightly inferior BER performance to that of conventional CAP in a multi-band system, but with computational complexity decreased below 10%. The BTN pulse is adopted because the side-lobes decay follows t^{-2}, where t is the instantaneous time sample, and the decay is faster than the SRRC case, whose side-lobes extend much further [11]. In this paper, we select these candidate pulse shapes as the basis function of the pulse shaping filters for the transmit and receive filters in CAP modulation. In the literature, it remains unclear whether the SRRC pulse offers optimal performance. Sequentially, we propose a new demodulation method outlined in Section II and then investigate the BER and error vector magnitude (EVM) performance of each VLC link when each format contains equivalent energy to maintain a fair test between the different pulses. We then provide insight into their respective performances by analysis of the eye diagrams at one sample-per-bit of both the in-phase and quadrature components following constellation de-mapping at the receiver. We find that the BTN-based system offers superior performance to the SRRC and Xia pulses in terms of BER, EVM, and similar performance in terms of the vertical and horizontal eye openings. Finally, we observe that the computational complexity of the proposed

BTN-based CAP system is lower than that of conventional CAP.

This paper is organised as follows. In Section II the experimental test setup is illustrated and described. Next, Section III describes the results and provides the discussion into the comparative BER performance of each pulse shape mentioned above. Finally, conclusions are drawn in Section IV.

II. Test Setup

A schematic block diagram of the test setup is shown in Fig. 1. A random data stream $\mathbf{D_s} = [d_{s0}, d_{s1}, \ldots, d_{sn}]$ is generated and mapped onto a quadrature amplitude modulation (QAM) constellation, and both 4-QAM and 16-QAM are tested in this work. The symbols are then up-sampled according to the number of samples-per-symbol (P/Q in Fig. 1) as described in [15] at a sampling frequency of $f_s = \lceil 2R_s(1+\beta) \rceil$, where β is the filter roll-off factor and R_s is the system baud rate, before being split into the real and imaginary components. Next, the constituent parts are shaped to form a Hilbert pair, meaning they occupy the same frequency range but are separated in phase by 90°. The three candidate pulses tested in this work are:

(*i*) the SRRC, given by:

$$g_S(t) = \frac{2\beta \left[\cos\left(\frac{(1+\beta)\pi t}{T_s}\right) + \sin\left(\frac{(1-\beta)\pi t}{T_s}\right) \left[\frac{4\beta t}{T_s}\right]^{-1} \right]}{\pi \sqrt{T_s} \left[1 - \left(\frac{4\beta t}{T_s}\right)^2 \right]} \quad (1)$$

where $T_s = 1/R_s$ is the symbol period and t is the instantaneous time sample.

(*ii*) the first-order Xia-pulse is defined as follows [9, 10]:

$$g_X(t) = \frac{\sin\left(\frac{\pi t}{T_s}\right) \cos\left(\frac{\pi \beta t}{T_s}\right)}{\left(\frac{\pi t}{T_s}\right)(2\beta t + T_s)} \quad (2)$$

(*iii*) the BTN pulse is given by [11]:

$$g_B(t) = \frac{\sin\left[\frac{\pi t}{T_s}\right] \left[\frac{2\pi \beta t}{T_s \ln(2)} \sin\left(\frac{\pi \beta t}{T_s}\right) + 2\cos\left(\frac{\pi \beta t}{T_s}\right) - 1 \right]}{\left(\frac{\pi t}{T_s}\right) \left[\left(\frac{\pi \beta t}{T_s \ln(2)}\right)^2 + 1 \right]} \quad (3)$$

For nomenclature, the use of the different pulses in the CAP system will be herein defined as conventional CAP, X-CAP and B-CAP for the SRRC, Xia and BTN pulses, respectively.

In order to form the Hilbert pair, these pulse shapes must be multiplied by the in-phase and quadrature carrier, to generate the final impulse response of the real and imaginary pulse shaping filters, $p(t)$ and $p'(t)$, respectively, as follows:

$$p(t) = g(t)\cos(2\pi f_c t) \quad (4)$$

$$p'(t) = g(t)\sin(2\pi f_c t) \quad (5)$$

where $g(t)$ is any of the three candidate pulse shapes, i.e. $g(t) = \{g_S(t), g_X(t), g_B(t)\}$, and f_c is the carrier frequency (set equal to R_s). The three candidate pulse waveforms with $\beta = 0.1$ after formation of the Hilbert pair can be seen in Fig. 2(a)—(c), where the black and red curves show the

in-phase and quadrature components, respectively. There are discrete differences between the three, where, in comparison to the well-known SRRC, the Xia pair are asymmetrical, with larger side-lobes on the left-hand side and slightly off-centre maxima, which is an important feature. The BTN-based pair are similar in shape to the SRRC, however with suppressed side-lobes. Both $p(t)$ and $p'(t)$ have a finite filter length L_s. As has been shown in the literature [13, 16], the effect of L_s can have a significant impact on the bit-error rate (BER) performance. As a result, we select several different values of L_s as described later in the section. In Fig. 3, the frequency responses for the three pulse shapes are shown.
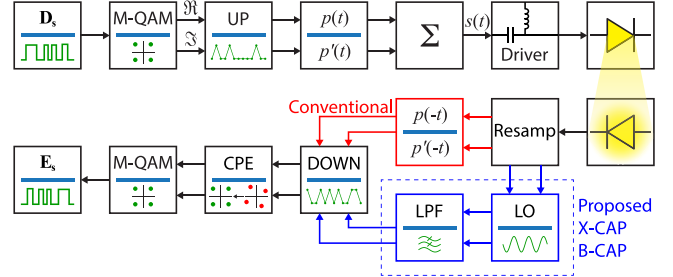

Fig. 1. Block diagram of the system under test.

After pulse shaping, the in-phase and quadrature data are summed in preparation for transmission via intensity modulation of a light-emitting diode (LED) over a typical additive white Gaussian noise (AWGN) VLC channel, where a direct line-of-sight is evident. The data is loaded into a Tektronix arbitrary function generator (AFG7122C) before being mixed with a 500 mA DC current via a bias tee with a ~30 kHz cut-on frequency to give the maximum possible symmetrical swing, thus enabling the highest possible signal-to-noise ratio (SNR). The LED used was an Osram Golden Dragon. The light-current and current-voltage (L-I-V) relationships of the LED are illustrated in Fig. 4 and high linearity can be seen for both. For further details of the transmitter including optical spectrum and SNR analysis, refer to [17]. The receiver consists of a Hamamatsu S5973 photodiode with an Analog Devices AD8015 transimpedance amplifier working in differential mode. The link distance was 10 cm and the received optical power was 1.5 mW measured using a ThorLabs PM100.

The total bandwidth offered was ∼ 2 MHz, seen in Fig. 5, which was measured using an Keysight N9020A MXA electrical spectrum analyser and a swept sine wave, without any equalisation techniques. Despite myriad reports of effective equalisation methods in the literature (i.e. [18]), we elected not to extend the bandwidth of the proposed system as we do not consider the impact of band-limitations in this work and as such, the overall data rate is not the focus of this work and can be set arbitrarily. Hence, we set the signal bandwidth to 1 MHz in order to ensure operation within the pseudo-flat portion of the system magnitude response and enable demodulation via a low-pass filter (LPF), in a similar manner to our previous work [13]. The reason that we opt against targeting a high transmission speed in this test is to investigate the performance of the proposed pulse shapes when adopted in non-band-limited VLC links. Each link was evaluated under
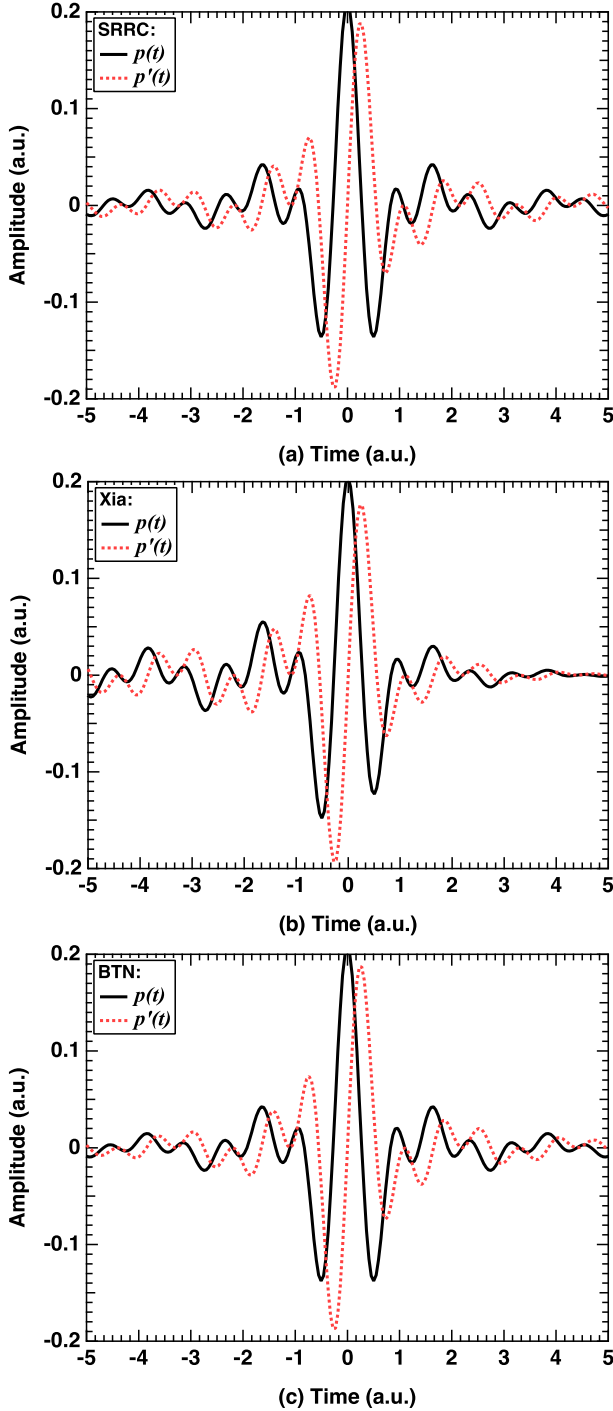
Fig. 2. Illustration of the three candidate pulses ((a) SRRC, (b) Xia and (c) BTN) after formation of the Hilbert pair by multiplication with the carrier.
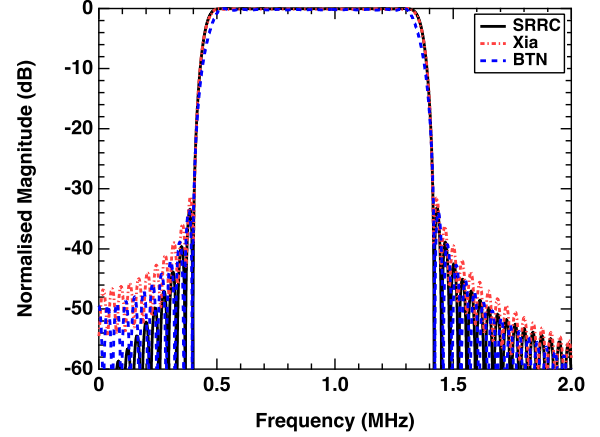

Fig. 3. The ideal frequency responses of the three candidate pulse shapes. Clearly the Xia and SRRC both have a slightly wider main-lobe, while the BTN offers a slightly more compact main-love while maintaining a low out-of-band emission similar to that of SRRC, both of which are lower than the Xia pulse.
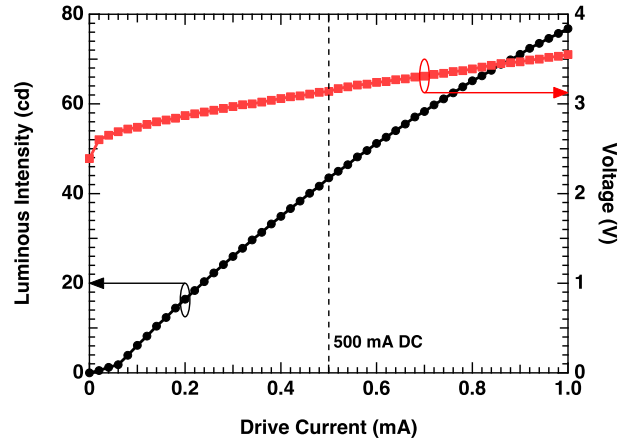

Fig. 4. Measured L-I-V curve for the LED under test.

the same conditions (i.e., bias, modulation, etc.) to provide a fair comparison.

Following photodetection and differential transimpedance amplification, the signal is sampled by a Tektronix MDO4054C real-time oscilloscope at a sampling frequency of 50 MS/s for offline digital signal processing in MATLAB. The first step is to resample the signal from the 50 MS/s rate back to the original pre-transmission sampling rate in Fig. 1. In the conventional method for CAP demodulation, matched filtering occurs where $p(-t)$ is the time-reversed matched filter for the in-phase component and $p'(-t)$ is the quadrature equivalent as indicated in the red blocks (see Fig. 1), followed by downsampling (i.e. Q/P) common phase error correction (CPE), constellation de-mapping and estimation of the symbols $\mathbf{E_s}$. In the proposed method, the first step is multiplication by a local oscillator to remove the carrier frequency and then using a tenth-order LPF with the cut-off frequency set to R_s to eliminate the signal image and out-of-band noise acquired through the receiver electronics and sampling stages. A 10th order filter was selected for two reasons; (*i*) to ensure significant attenuation of any signal harmonics beyond the filter cut-off frequency; and (*ii*) for consistency with our previous work [14]. After the LPF, the received signals are passed through the time-reversed matched filters (quadrature), before downsampling and constellation de-mapping in order to provide estimates of the received symbols and bits, respectively.

In this work we investigate the BER and EVM performance of each candidate pulse shape for both 4- and 16-QAM and
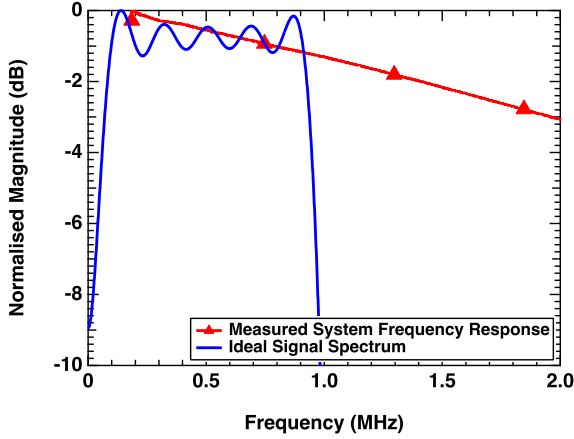
Fig. 5. Measured frequency response for an SRRC signal under test and the system frequency response, simulated frequency response of the bias-tee used to modulate the information onto the DC bias.

provide a detailed analysis of the eye diagrams of each in terms of both the vertical and horizontal eye openings. This will give insight into the best performing pulse shape for CAP modulation within the context of a VLC system free of band-limitations. Furthermore, we study the impact of varying the filter length on each pulse shape and its consequential effect on the performance metrics investigated. As pulse shaping filter lengths are shortened, the number of side-lobes truncated increases and hence, the ISI increases due to the lower filter quality. We investigate filter lengths L_s spanning from 4 symbols up to 16 symbols in steps of 4. For the entirety of this work, $\beta = 0.1$, which forces more energy into the side-lobes than any β commonly found in the literature [2, 4, 9, 11, 15], and will have the largest impact on the BER.

III. RESULTS

Firstly, insight can be gained by analysis of the eye diagram's vertical and horizontal characteristics. We elect to measure the vertical (ΔA) and horizontal (Δt) eye openings, as illustrated in Fig. 6. The eye diagrams are measured after down-sampling to one sample-per-bit and since complex modulation is used, an eye diagram is produced for both the quadrature and in-phase components of the signal, and statistics are extracted for both parts.

In Fig. 7(a)–(b), the vertical eye openings for the in-phase and quadrature components and 4-QAM modulation are shown, respectively. Starting with Fig. 7(a), it is clear that the in-phase vertical eye opening increases with the filter length L_s for each of the candidate pulses albeit with varying gradients. The eye openings of each pulse increase with increasing L_s, as would be expected for the SRRC, which shows $\Delta A = 0.9$ V for $L_s = 4$, increasing to ~ 1.3 V for $L_s = 16$, increasing the opening by approximately $\sim 40\%$. This results in reduced ISI due to the inclusion of more of the impulse response side-lobes and hence, the BER and EVM are both reduced as demonstrated in Figs. 8 and 9. Relative to the SRRC case, the vertical eye openings for the B- and X-CAP systems are less dependent on the filter length, only increasing from around 1.15 V and 1 V when $L_s = 4$, respectively. Varying the filter

length by 400% to $L_s = 16$, the eye opening only changes by $\sim 10\%$, while the SRRC changes by $\sim 45\%$. Again, the voltage penalty experienced by the X-CAP system in comparison to the B-CAP system is attributed to the asymmetry of the Xia pulse peak, and the same trends as previous are observed, where the SRRC and BTN pulses closely converge to the same vertical eye opening. The same evaluation is performed for the quadrature component of the downsampled signal, as illustrated in Fig. 7(b), and the same patterns emerge albeit with a slightly different shape.

In Fig. 7(c)–(d), the horizontal eye openings for the in-phase and quadrature components are shown. Firstly, Fig. 7(c) depicts the horizontal eye openings (i.e. Δt from Fig. 6) for the in-phase component of the downsampled data for the three candidate pulses. Again, beginning with BTN, which demonstrates the best performance, where $\Delta t =\sim 0.8$ μs for $L_s = 4$. This increases in a pseudo-linear manner as previously observed for the vertical eye openings to a maximum $\Delta t =\sim 0.9$ μs. This means that increased tolerance to jitter is expected to be achieved due to the larger horizontal opening. Having a wide horizontal eye opening is preferential because it enables protection against random and deterministic jitter as the sensitivity to sampling-offset error is reduced, which has been a criticism of CAP modulation in the literature [15].

The BTN and Xia pulses demonstrate similar horizontal eye opening features, increasing slightly from ~ 0.8 μs (in-phase) and ~ 0.75 μs (quadrature) for $L_s = 4$ to ~ 0.9 μs for $L_s = 16$. As will be seen for the horizontal eye opening of the quadrature component, a similar trend is observed for all three pulses, which is interesting because there is little difference between the horizontal performance of the BTN and Xia pulses. Hence, this reinforces that the difference in BER between B-CAP and X-CAP can be attributed to the offset peak of the Xia pulse, which makes it inferior to that of the BTN overall.

Next, the EVM and BER performance of the three candidate pulse shapes will be discussed. A total of 10^7 bits were transmitted and hence the BER target is set to 10^{-6}. Fig. 8 highlights the BER results for each candidate pulse shape as a
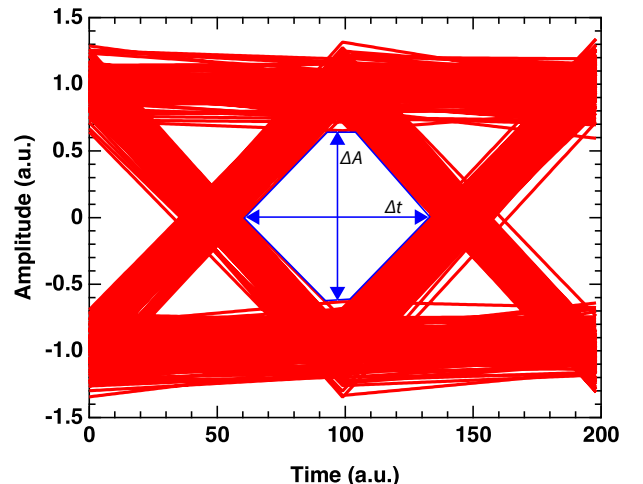

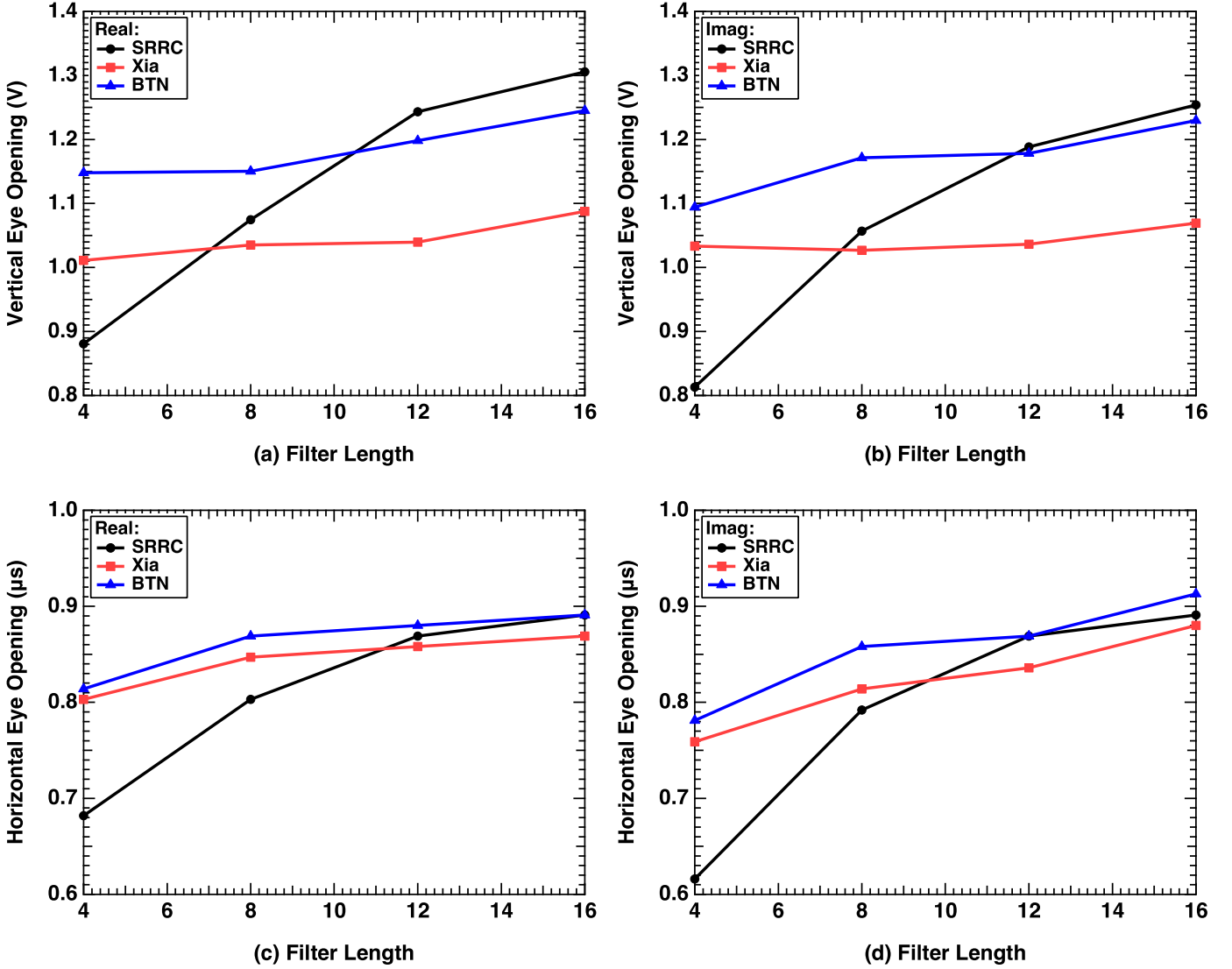Fig. 6. An illustration of the key performance indicators under test.

Fig. 7. Eye diagram key performance indicators for (a) in-phase and (b) quadrature signal components considering the vertical eye opening, and (c) in-phase and (d) quadrature signal components considering the horizontal eye opening.

function of the filter length L_s for the 16-QAM constellation. Considering a 1 MHz signal bandwidth and $\beta = 0.1$, the baud rate of the system is given as $R_s = B_{signal}/(1 + \beta) = 0.91$ MBd/s [15] and is kept constant for both 4- and 16-QAM. It is clear from observation that the SRRC-based CAP BER performance is heavily dependent on L_s, reducing from $\sim 10^{-2}$ for $L_s = 4$ to 2×10^{-7} for $L_s = 16$. Interestingly, for the full Nyquist configuration (i.e. conventional CAP) without matched filters, the same pattern is observed but is far less severe. Only a marginal BER improvement is observed for both the BTN and Xia pulses, where the BER of 2×10^{-4} at $L_s = 4$ is improved to $\sim 5 \times 10^{-5}$ for a filter length of 16. Similarly, for BTN pulses, for $L_s = 4$ symbols, a BER of 10^{-5} can be immediately achieved, improving to 2×10^{-7} at the full 16-symbol filter span.

It is noteworthy that both the Xia and BTN pulses outperform the SRRC for low FIR filter lengths. The reason for this is because the entire system becomes less dependent on the side-lobes when considering a full-Nyquist configuration and more dependent on the peak horizontal opening of the pulse, which is always in the centre of the filter impulse response. Hence, filter truncation has little impact, particularly when considering matched filtering, such that the effect of the truncation must be considered once at the transmitter and once at the receiver. Interestingly, the X-CAP format shows a BER penalty for $L_s > 8$ and this has also been noted in other work [14, 19] and is rooted in the fact that the peak of the Xia pulse is offset from the centre, hence causing a power penalty that leads to a reduction in BER. This is particularly evident when considering that the BTN and SRRC pulses converge on the same BER value for a filter length of 16. Inset in Fig. 8, the intensity-mapped constellations are illustrated for each pulse shape for $L_s = 4$ and 16, highlighting the differences (SRRC) and similarities (Xia and BTN) across the filter lengths tested. It should be noted that for 4-QAM, the BER floor was met for each pulse shape for every value of L_s and hence, these results are omitted from Fig. 8.

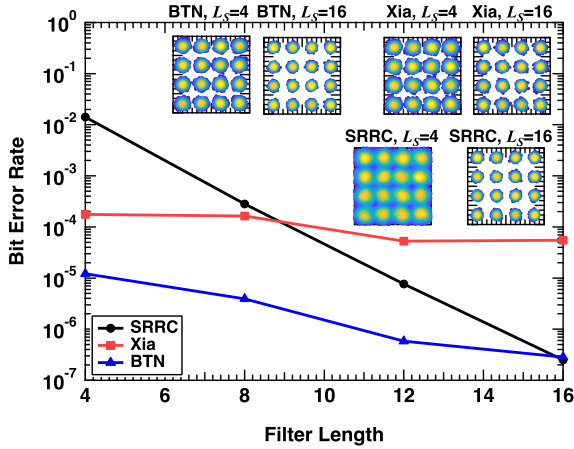The EVM performance for both 4- and 16-QAM are shown

Fig. 8. BER performance for the three candidate pulses using 16-QAM. Inset are constellation diagrams that illustrate the performances of the different configurations for $L_s = 4$ and 16 .
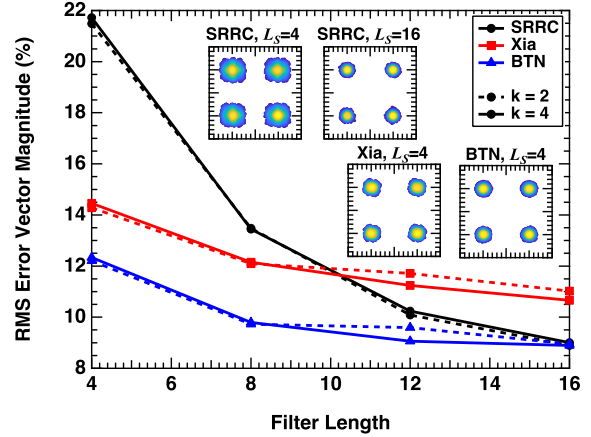

Fig. 9. Error vector magnitude for both 4-QAM and 16-QAM for each of the three candidate pulses under test, constellation diagrams shown inset are for $L_s = 4$, and also for $L_s = 12$ in the case of the conventional SRRC-based system.

in Fig. 9. A similar EVM profile can be observed for both 4-QAM (dashed) and 16-QAM (solid) for each candidate pulse shape, corresponding to superior BER performance for 4-QAM as reported in the literature [20] and Fig. 8. As expected, based on the BER results previously shown, the EVM values for the X-CAP and B-CAP configurations significantly outperform those of conventional CAP at low filter lengths, advantageously reducing them to approximately 14% and 12%. As was shown in the BER case, the EVM curves follow the same trend, where convergence to the same EVM value is achieved for both B-CAP and the conventional case, while X-CAP shows a slight penalty according to its offset peak as mentioned. The inset in Fig. 9 depicts the intensity-mapped constellations for all three candidate pulses modulated by 4-QAM and $L_s = 4$ and for $L_s = 12$ in the case of SRRC, specifically to highlight the difference in quality. Clearly, the results obtained for both the BER and EVM are as expected based on the observed vertical and horizontal eye openings. No improvement in either BER or EVM is obtained for $L_s > 16$.

A. Comments on Computational Complexity

The computational complexity of CAP systems is crucial for their use in high speed communication systems, since they could require a significant number of FIR filters, i.e. increased complexity. Previously, 4 FIR filters were used for a single subcarrier CAP system; two required at the transmitter and two at the receiver. In [21] it was shown that the transmit pair can be removed and replaced with look-up tables within a real-time processor such as field programmable gate array (FPGA), thus reducing the filter requirement to 2. In the following equations, the complexity is linked to the Baud rate, R_s, to link to real time development at higher transmission speeds. It should be noted that the common phase error (CPE) is constant in both systems and hence omitted from the calculations but is considered in [22]. Taking this into account, the computational complexity for conventional CAP using 2 FIR filters, measured

in real-valued multiplications-per-second is given be [14, 22]:

$$C = R_s \left(2 + 2M_N L_s\right) \tag{6}$$

where M_N is the number of samples-per-symbol. Clearly, C increases linearly with either M_N or L_s. For the $L_s = 16$ system used here, $M_N = 6$ and hence, the number of real-valued operations-per-second was $194R_s$. In the proposed method, using either B-CAP or X-CAP, both of which do not have a matched filter at the receiver, but instead a 10th order LPF, the complexity becomes [14]:

$$C = 2R_s L_s \tag{7}$$

where $L_s = 11$ for a 10th order LPF, and hence, for either the B-CAP or X-CAP system operating at the equivalent conditions as the previous case, the computational complexity is significantly reduced to $22R_s$, which translates into over an eight-fold decrease in computational complexity. This is important, as not only can one obtain significantly improved BER results with shorter filter lengths in comparison to the traditional system, the computational complexity can also be significantly reduced.

IV. CONCLUSION

In this paper we proposed, for the first time, the BTN and Xia pulses to complement the typical SRRC that is traditionally employed in VLC and CAP in general as the Hilbert pair impulse response basis function of the transmit and receive filters, introducing B-CAP and X-CAP. We have experimentally investigated the comparative BER and EVM performances of the two new pulses with the SRRC pulse, alongside the vertical and horizontal eye openings for different filter lengths. We clearly show that both the B-CAP and X-CAP VLC system offer superior BER performance at short filter lengths, which simultaneously lowers the system computational complexity by around 8 times.

Acknowledgment

References

[1] D. Tsonev, H. Chun, S. Rajbhandari, J. J. D. McKendry, S. Videv, E. Gu, M. Haji, S. Watson, A. E. Kelly, G. Faulkner, M. D. Dawson, H. Haas, and D. O'Brien, "A 3-Gb/s single-LED OFDM-based wireless VLC link using a gallium nitride μLED," *IEEE Photonics Technology Letters*, vol. 26, no. 7, pp. 637–640, April 2014.

[2] F. M. Wu, C. T. Lin, C. C. Wei, C. W. Chen, Z. Y. Chen, H. T. Huang, and S. Chi, "Performance comparison of OFDM signal and CAP signal over high capacity RGB-LED-based WDM visible light communication," *IEEE Photonics Journal*, vol. 5, no. 4, pp. 7 901 507–7 901 507, Aug 2013.

[3] S. Rajbhandari, J. J. McKendry, J. Herrnsdorf, H. Chun, G. Faulkner, H. Haas, I. M. Watson, D. OBrien, and M. D. Dawson, "A review of gallium nitride LEDs for multi-gigabit-per-second visible light data communications," *Semiconductor Science and Technology*, vol. 32, no. 2, p. 023001, 2017.

[4] P. A. Haigh, A. Burton, K. Werfli, H. L. Minh, E. Bentley, P. Chvojka, W. O. Popoola, I. Papakonstantinou, and S. Zvanovec, "A multi-CAP visible-light communications system with 4.85-b/s/Hz spectral efficiency," *IEEE Journal on Selected Areas in Communications*, vol. 33, no. 9, pp. 1771–1779, Sept 2015.

[5] J. Wei and E. Giacoumidis, "Multi-band CAP for Next-Generation Optical Access Networks Using 10-G optics," *Journal of Lightwave Technology*, vol. 36, no. 2, pp. 551–559, 2018.

[6] J. Wei, Q. Cheng, D. G. Cunningham, R. V. Penty, and I. H. White, "100-Gb/s hybrid multiband CAP/QAM signal transmission over a single wavelength," *Journal of Lightwave Technology*, vol. 33, no. 2, pp. 415–423, 2015.

[7] A. F. Shalash and K. K. Parhi, "Multidimensional carrierless AM/PM systems for digital subscriber loops," *IEEE Transactions on Communications*, vol. 47, no. 11, pp. 1655–1667, Nov 1999.

[8] D. Falconer, "Carrierless AM/PM," *Bell Laboratories, NJ, USA, Bell Laboratories Technical Memorandum, Tech. Rep*, 1975.

[9] M. Tavan, E. Agrell, and J. Karout, "Bandlimited intensity modulation," *IEEE Transactions on Communications*, vol. 60, no. 11, pp. 3429–3439, November 2012.

[10] X.-G. Xia, "A family of pulse-shaping filters with ISI-free matched and unmatched filter properties," *IEEE Transactions on Communications*, vol. 45, no. 10, pp. 1157–1158, Oct 1997.

[11] N. C. Beaulieu, C. C. Tan, and M. O. Damen, "A "better than" Nyquist pulse," *IEEE Communications Letters*, vol. 5, no. 9, pp. 367–368, Sept 2001.

[12] P. Chvojka, P. A. Haigh, S. Zvanovec, P. Pesek, and Z. Ghassemlooy, "Evaluation of multi-band carrier-less amplitude and phase modulation performance for VLC under various pulse shaping filter parameters," in *Proceedings of the 13th International Joint Conference on e-Business and Telecommunications (ICETE 2016)*, 2016, pp. 25–31.

[13] P. Chvojka, K. Werfli, S. Zvanovec, P. A. Haigh, V. H. Vacek, P. Dvorak, P. Pesek, and Z. Ghassemlooy, "On the m-CAP performance with different pulse shaping filters parameters for visible light communications," *IEEE Photonics Journal*, vol. 9, no. 5, pp. 1–12, Oct 2017.

[14] P. A. Haigh and I. Darwazeh, "Demonstration of reduced complexity multi-band CAP modulation using Xia-pulses in visible light communications," in *Optical Fiber Conference (OFC)*, 2018.

[15] M. I. Olmedo, T. Zuo, J. B. Jensen, Q. Zhong, X. Xu, S. Popov, and I. T. Monroy, "Multiband carrierless amplitude phase modulation for high capacity optical data links," *Journal of Lightwave Technology*, vol. 32, no. 4, pp. 798–804, Feb 2014.

[16] P. Chvojka, P. A. Haigh, S. Zvanovec, P. Pesek, and Z. Ghassemlooy, "Evaluation of multi-band carrier-less amplitude and phase modulation performance for VLC under various pulse shaping filter parameters," in *OPTICS*, 2016, pp. 25–31.

[17] P. A. Haigh, Z. Ghassemlooy, S. Rajbhandari, I. Papakonstantinou, and W. Popoola, "Visible light communications: 170 Mb/s using an artificial neural network equalizer in a low bandwidth white light configuration," *Journal of Lightwave Technology*, vol. 32, no. 9, pp. 1807–1813, May 2014.

[18] X. Huang, Z. Wang, J. Shi, Y. Wang, and N. Chi, "1.6 Gbit/s phosphorescent white LED based VLC transmission using a cascaded pre-equalization circuit and a differential outputs PIN receiver," *Opt. Express*, vol. 23, no. 17, pp. 22 034–22 042, Aug 2015.

[19] C. C. Tan and N. C. Beaulieu, "Transmission properties of conjugate-root pulses," *IEEE Transactions on Communications*, vol. 52, no. 4, pp. 553–558, April 2004.

[20] R. Schmogrow, B. Nebendahl, M. Winter, A. Josten, D. Hillerkuss, S. Koenig, J. Meyer, M. Dreschmann, M. Huebner, C. Koos, J. Becker, W. Freude, and J. Leuthold, "Error vector magnitude as a performance measure for advanced modulation formats," *IEEE Photonics Technology Letters*, vol. 24, no. 1, pp. 61–63, Jan 2012.

[21] J. Wei, C. Sanchez, P. A. Haigh, and E. Giacoumidis, "Complexity comparison of multi-band CAP and DMT for practical high speed data center interconnects," in *Asia Communications and Photonics Conference*. Optical Society of America, 2017, pp. M2G–4.

[22] J. Wei, J. Ingham, Q. Cheng, D. Cunningham, R. V. Penty, and I. H. White, "High performance optical data links using hybrid CAP/QAM transmitter/receiver scheme," in *Asia Communications and Photonics Conference 2013*. Optical Society of America, 2013, p. AW4G.1.